The Stochastic Search Dynamics of Interneuron Migration

Joanne M. Britto,[†] Leigh A. Johnston,[†‡] and Seong-Seng Tan[†*]
[†]Howard Florey Institute, Florey Neuroscience Institutes, and Centre for Neuroscience, and [‡]NICTA Victoria Research Laboratory, Department of Electrical & Electronic Engineering, University of Melbourne, Melbourne, Australia

ABSTRACT Migration is a dynamic process in which a cell searches the environment and translates acquired information into somal advancement. In particular, interneuron migration during development is accomplished by two distinct processes: the extension of neurites tipped with growth cones; and nucleus translocation, termed nucleokinesis. The primary purpose of our study is to investigate neurite branching and nucleokinesis using high-resolution time-lapse confocal microscopy and computational modeling. We demonstrate that nucleokinesis is accurately modeled by a spring-dashpot system and that neurite branching is independent of the nucleokinesis event, and displays the dynamics of a stochastic birth-death process. This is in contrast to traditional biological descriptions, which suggest a closer relationship between the two migratory mechanisms. Our models are validated on independent data sets acquired using two different imaging protocols, and are shown to be robust to alterations in guidance cues and cellular migratory mechanisms, through treatment with brain-derived neurotrophic factor, neurotrophin-4, and blebbistatin. We postulate that the stochastic branch dynamics exhibited by interneurons undergoing guidance-directed migration permit efficient exploration of the environment.

INTRODUCTION

Knowledge of the cellular mechanisms involved in migration is fundamental in understanding a number of disease states that arise from the failure or dysregulation of such processes (1,2). Neurons display migratory behaviors characterized by the extension of neurites tipped with highly motile growth cones that sense guidance cues and transmit intracellular signals to produce somal translocation (3,4). Extensive research has been undertaken to understand the ability of a neuronal growth cone to navigate and respond to attractive and repulsive cues (see reviews by (5,6)); however, the manner in which interactions with the environment crystallize into neuronal movement remains an area of active research.

Migration is a key component of cortical development as neuronal progenitors arise in locations distal to where the fully differentiated neurons reside. The majority of neurons in the cortex—excitatory projection neurons—are generated locally in the ventricular germinal zones, and use radial glia to guide migration (7). In contrast, inhibitory interneurons are generated outside of the cortex in the developing striatum and rely on biochemical cues in the surrounding milieu to reach the developing cortical plate (8–11). Unlike olfactory interneurons in the rostral migratory stream that migrate in chains (12), the individual searching behavior of cortical interneuron migration is evidenced in vigorous and dynamic neurite branching, and in the intermittent leaps made by the nucleus to advance the cell, termed nucleokinesis (13). Although saltatory nuclear translocation and dynamic branch extension and retraction have been noted (13,14), a study of the precise nature of the relationship between these two fundamental components of interneuron migration has not been undertaken. The primary objective of this article is to mathematically model neurite branching and nucleokinesis to better understand the interplay between the mechanisms of migration.

Cell migration has been studied using a variety of approaches across a range of spatial and temporal scales. The study of the spatial trajectories of motile cells, relating cellular responses to molecular gradients and substrate perturbations, termed taxis, is most often analyzed using the tools of stochastic calculus, random walks, and diffusion processes (15–20). In contrast, bottom-up biomechanical models of cell adhesion, protrusion, and retraction have been proposed that quantitatively describe defined mechanisms of motion (21), as a function of factors such as proteins levels marked by local pH value (22) and actin-myosin density (23). Validation of a mathematical model of cell migration demands an experimental paradigm that permits manipulation while maintaining as close to a realistic environment as possible. We therefore chose to study organotypic cortical slice cultures, which can be imaged using time-lapse confocal microscopy. Although it is known that migrating neurons are attracted to certain molecular guidance cues and are repelled by others (24), the recent work of Martini et al. (25) is the first to study the neurite branching response of interneurons to chemoattractant signals. Their qualitative results suggest a role for the orientation of the leading neurite branch in navigating a chemoattractant gradient and highlight the relevance of branching dynamics to guidance-directed migration.

Quantitative modeling of neurite branch dynamics has largely focused on axon guidance in postmigratory neurons from, for example, the continuum models of neurite growth as a function of intracellular factors including tubulin concentration (26) and intracellular calcium concentration (27). Functions of extracellular cues have similarly been

Submitted January 21, 2009, and accepted for publication April 28, 2009.

Joanne M. Britto and Leigh A. Johnson contributed equally to this work.

*Correspondence: stan@florey.edu.au

Editor: Alexander Mogilner.

0006-3495/09/08/0699/11 $2.00

doi: 10.1016/j.bpj.2009.04.064

modeled; for example, the stochastic and deterministic behaviors of growth cone pathfinding subject to attractive and repulsive substrate guidance cues (28), and models of axonal chemotaxis that can replicate empirical growth cone navigation data (29). The migrating interneuron involves growth cone guidance, with the additional complexity of nuclear locomotion and its relationship to the search dynamics of the branches.

Using high-resolution time-lapse confocal microscopy, we have studied the pioneering population of interneurons that migrate into the embryonic cortex. We utilized a 5-min interframe imaging protocol, necessary to capture the fast dynamics of neurite branches. Our results demonstrate that a stochastic birth-death model of neurite branching accurately and robustly accounts for the observed branch dynamics. Models similar to the birth-death model we posit here have been applied elsewhere in the biological domain (30), for endothelial cell locomotion (31) and for modeling the dynamics of the actin filament network associated with lamellipodia extension (32). Concomitant to demonstrating the stochasticity of the neurite branch dynamics, we conclude that the temporal dynamics of branching can be considered separately from the events of nucleokinesis. Our results lead us to hypothesize that the highly dynamic branching employed by migrating interneurons is conceptually analogous to a stochastic search algorithm, in which an unknown environment is efficiently searched through directed, yet random, exploration.

METHODS

Time-lapse imaging of organotypic slice cultures

Experiments were undertaken with the approval of the Howard Florey Institute Animal Ethics Committee and conform to the Australian Code of Practice for the Care and Use of Animals for Scientific Purposes (seventh edition, 2004). Organotypic slice cultures of embryonic day 12.5 embryos were prepared using glutamic acid decarboxylase 67 knock-in green fluorescent protein mice ($GAD67^{GFP/+}$) as previously described (33). Media was supplemented with 100 ng/mL recombinant human brain-derived neurotrophic factor or 100 ng/mL recombinant human neurotrophin-4 (kind gift from Dr X. Fu) or 70–100 μM blebbistatin (Tocris Bioscience, Ellisville, MO) for the entire duration of the culture. Interneurons positive for GFP were imaged on an inverted Axiovert 200-LSM5 Pascal confocal microscope (Zeiss, Oberkochen, Germany). All images were captured using a 10× objective (2× digital zoom) and an optical slice $<10\ \mu$m. Two time-lapse protocols were used for image acquisition: 5-min intervals for up to 4 h in a 37°C, 5% CO_2 humidified stage incubator, and 30-min intervals for which cultures were incubated at 37°C, 5% CO_2 and placed at room temperature for imaging.

Neuron tracking

The initial population of interneurons migrating with branches visible for >15 time-intervals was tracked using in-house software developed in MATLAB (The MathWorks, Natick, MA). The position of the nucleus center-of-mass at each frame, $\mathbf{x}_t = (x_t, y_t)$, was recorded at time instants $t = 0, \Delta_t, 2\Delta_t, \ldots, T$, where Δ_t is the imaging interval and T is the total imaging time. The neuron morphology was manually delineated at each frame to indicate the position of all branches and branch-points. Unique identifiers were given to each branch and branch-point, which allowed tracking through the image sequence with respect to parent branch-points and sibling branches. Branches tipped and not tipped by active growth cones were not differentiated.

The onset and offset times, t_{on} and t_{off}, of each nucleokinesis event for each neuron were manually recorded via the tracking software. A nucleokinesis onset was declared when a previously stationary nucleus made a movement in one interframe interval that exceeded the background level of interframe positional disturbance. The nucleokinesis offset was marked as the frame at which the nucleus' interframe movement ceased.

Model of branch dynamics

Interarrival times of branches for each interneuron and the lifespan of each individual branch were calculated from the tracked data. Exponential probability density functions (pdfs) were fit to the resultant interarrival time and lifespan histograms. The interarrival time, $u > 0$, was parameterized by rate, λ,

$$p(u) = \lambda e^{-\lambda u}. \tag{1}$$

The reciprocal of the rate, $1/\lambda$, is the average interarrival time of the branches. Similarly, the branch lifespan, $v > 0$, was parameterized by rate, μ,

$$p(v) = \mu e^{-\mu v}. \tag{2}$$

Here the reciprocal of the rate, $1/\mu$, is the average lifespan of the branches.

Continuous-time, discrete-state, Markov chain models of branch dynamics, equivalently termed birth-death processes, were formulated to model the interneuron branch dynamics. For each birth-death model, the system state at time t was defined to be the number of branches in the neuritic arbor at time t, with transition probabilities between states determined by birth and death rates. The birth rate of a birth-death process is associated with the Markov chain's forward transition probabilities, and is given by the parameter, λ, of the interarrival distribution, Eq. 1. The death rate is associated with the Markov chain's backward transition probabilities, and is given by the parameter, μ, of the lifespan distribution, Eq. 2. Determining the functional form of these associations among λ, μ, and the Markov chain transition probabilities is the art of modeling the system. Various birth-death models of the interneuron branch dynamics are hypothesized and tested in Results.

Model of nucleokinesis dynamics

The dynamics of the interneuron nucleus during nucleokinesis were modeled by a mass-spring-dashpot system, where the mass of each nucleus was assumed to be equal. Displacement of the nucleus was measured by accumulated distance, r_t, during the nucleokinesis event from the marked onset frame at time t_{on} (accumulated distance zero) to the marked offset frame at time t_{off}. That is, for any time t during nucleokinesis,

$$\begin{aligned} r_t &= \|\mathbf{x}_t - \mathbf{x}_{t-\Delta_t}\| + r_{t-1}, \\ t &= \{t_{on} + \Delta_t, t_{on} + 2\Delta_t, \ldots, t_{off}\}, \end{aligned} \tag{3}$$

where Δ_t is the imaging interval. Accumulated distance is equivalent to the straight-line distance from initial position, as during nucleokinesis, the nucleus movement is linear.

The spring-dashpot system, equivalently a second-order damped harmonic oscillator, is

$$\ddot{r}_t + c\dot{r}_t + kr_t = 0, \tag{4}$$

where k is the spring constant, c the damping factor, and here subscript t indexes continuous time.

The spring-dashpot response, derived by solving Eq. 4 subject to boundary conditions, $r_{t_{on}} = 0$ at nucleokinesis onset, $r_{t_{off}}$ at nucleokinesis offset, and initial velocity estimate $\dot{r}_{t_{on}}$, is given by

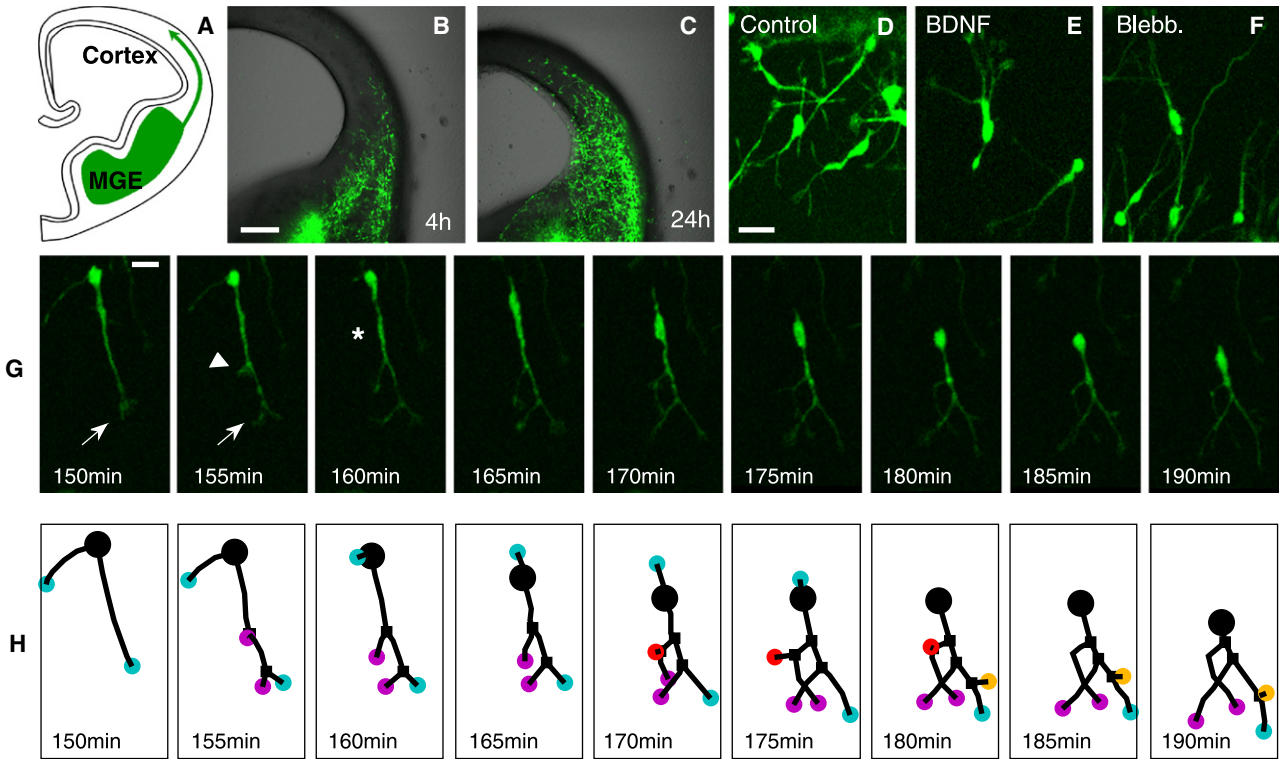

FIGURE 1 Migratory behaviors of cortical interneurons. (*A*) Schematic depicting migration of interneurons from the medial ganglionic eminence (MGE) into the cortex. Organotypic slices of E12.5 GAD67$^{GFP/+}$ cortex at (*B*) 4 h and (*C*) 24 h in culture. (*D*) Images of control, (*E*) BDNF, and (*F*) blebbistatin-treated interneurons show changes in cellular morphology. (*G*) Time-lapse sequence of migrating interneuron taken at 5-min intervals. (*H*) Schematic of tracked time-lapse sequence showing nucleus (*black circle*), branches (*color circle*), and branch points (*black square*). Each branch is assigned a color to represent the hierarchy of origin. Scale bars: (*B* and *C*) 200μm; (*D–G*) 20 μm.

$$r_t = r_{t_{\text{off}}}(1 - e^{\gamma_1 t}) - \frac{\gamma_1 r_{t_{\text{off}}} + \dot{r}_{t_{\text{on}}}}{\gamma_2 - \gamma_1}(e^{\gamma_1 t} - e^{\gamma_2 t}), \qquad (5)$$

where $c = -(\gamma_1 + \gamma_2)$ and $k = c^2/((\gamma_2 - \gamma_1)^2 + 4)$. For each nucleokinesis event, the parameters k and c were estimated by a nonlinear least-squares fit of the accumulated distance to the time response in Eq. 5.

Statistical analysis

Empirical pdfs were formed from histograms by normalizing the area under the histograms to one, thus transforming frequency to probability. The two-sample Kolmogorov-Smirnov test was applied to the null hypothesis of equal cumulative distribution functions. The null hypothesis of equal group medians was tested via the Kruskal-Wallis nonparametric one-way ANOVA test. Hotelling's T-square test was used to test the null hypothesis that the estimated spring-dashpot parameters were equal between control and treatment. The time interval between a nucleokinesis event and subsequent branch birth was tested for memorylessness by a Kolmogorov-Smirnov test of an exponential fit of the observed intervals. A similar test was applied to the interval between a nucleokinesis event and subsequent branch death.

RESULTS

Interneuron migration during cortical development

To observe the manner in which interneurons migrate, we performed time-lapse imaging of slice cultures obtained from GAD67$^{GFP/+}$ mice (34). Organotypic cultures of embryonic day 12.5 embryos show GFP expressed by interneurons generated in the medial ganglionic eminence, and migration into the naïve cortex after 24 h (Fig. 1, *A–C*). The processes by which interneurons migrate are consistent with established rules of neuronal migration (35). Initially, a leading branch capped by a growth cone extends in the direction of migration (*arrow*, Fig. 1 *G*). New branches are created by the formation of a new growth cone (*arrowhead*, Fig. 1 *G*) or division of the leading growth cone to generate a pair of branches (*arrow*, Fig. 1 *G*). Subsequent cytoplasmic dilation in the leading branch immediately ahead of the nucleus is observed before translocation of the nucleus (*asterisk*, Fig. 1 *G*). We tracked the location of each branch and branch-point through the image sequences, recording the hierarchical arrangement of the neuritic arbor through time (Fig. 1 *H*, Movie S1 in the Supporting Material). Our observations confirm previous findings (8,13) that migrating interneurons display repeated rounds of branch extension and retraction, accompanied by sudden leaps in nuclear position (Movie S2).

The stochastic nature of branch dynamics

Our observations of interneuron branching lead to the hypothesis that the dynamics of the neuritic arbor are well modeled by a birth-death process. The birth process is

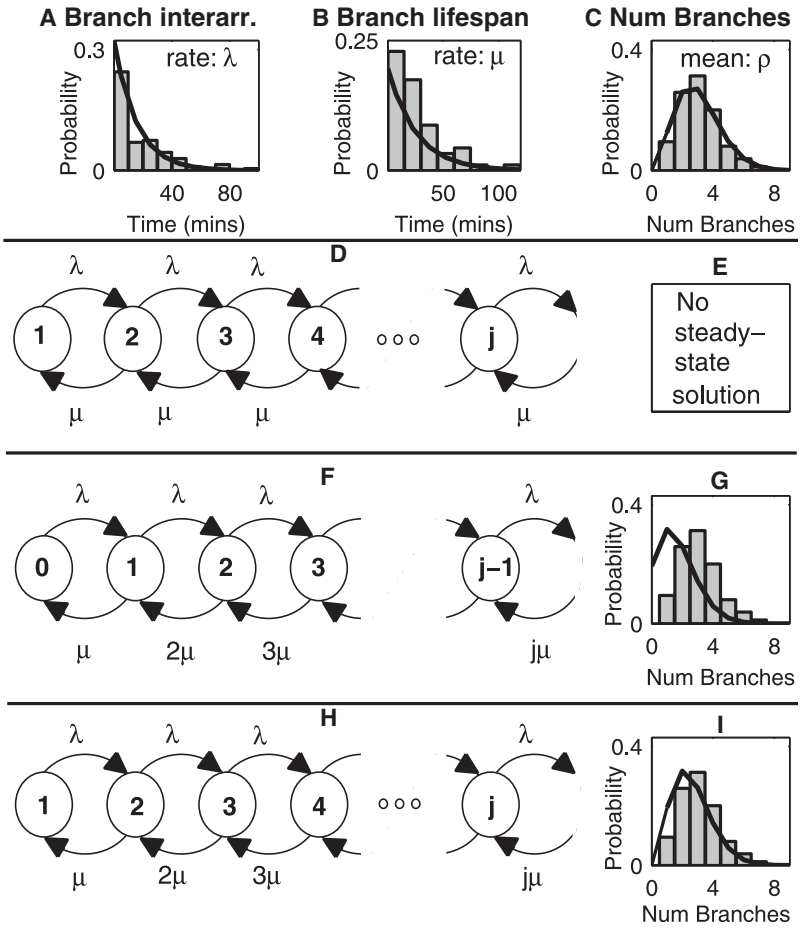

FIGURE 2 Stochastic dynamics of neurite branching in control interneurons. (*A*) Histogram of branch interarrival times and best-fit exponential pdfs (Eq. 1, *solid lines*). (*B*) Histogram of branch lifespans and best-fit exponential pdfs (Eq. 2, *solid lines*). (*C*) Histogram of neuritic arbor size overlaid by empirically derived shifted Poisson distribution (Eq. 10, *solid line*) parameterized by ρ_e, corresponding to the model in panel *I*. Hypothesized models of neuritic arbor dynamics: (*D*) ordained branch retraction model in which only one branch is available for the next retraction (equivalently a single-server queue). (*E*) No steady-state distribution exists as $\lambda/\mu > 1$ for control interneurons (see Table 1). (*F*) Unrestricted branch retraction model (equivalently a multiserver queue). (*G*) Histogram of neuritic arbor size overlaid by steady-state Poisson distribution (Eq. 8, *solid line*) parameterized by $\widehat{\rho}$. (*H*) Restricted branch retraction model, based on the observation that migrating interneurons always display one or more branches. (*I*) Histogram of neuritic arbor size overlaid by steady-state-shifted Poisson distribution (Eq. 10, *solid line*) parameterized by ρ_m (Eq. 11).

defined by the time interval between two consecutive branch births, termed the branch interarrival time. The death process is defined by the length of time for which a branch exists, termed the branch lifespan. Empirical distributions of branch interarrival times and branch lifespans in the neuritic arbors of control neurons ($n = 17$) are displayed in Fig. 2, panels *A* and *B*, respectively.

The memoryless property of branch interarrivals and lifespans is demonstrated by the fit of exponential distributions to each of the empirical pdfs, shown as solid lines in Fig. 2 (see Methods for optimization details). The interarrival rate parameter, λ, is the birth rate of the branches. The lifespan rate parameter, μ, is the death rate. The reciprocal of the rates, $1/\lambda$ and $1/\mu$, define the average interarrival time and average lifespan, respectively. Estimated values for λ and μ for the control interneurons, derived from the best fit exponential distributions, are listed in Table 1.

The accurate description of branch interarrival and lifespan dynamics by exponential distributions leads to the formulation of the temporal population branch dynamics as a continuous-time, discrete-state Markov chain model. The state of the Markov chain at time t is the number of branches in the neuritic arbor at that time, indicated by nodes in a state diagram. We hypothesize three models that may be reasonably expected to describe the dynamics of the neuritic arbor, and demonstrate that only one of the three models reflects the experimental data.

The first model encapsulates the hypothesis that at any point in time, there is a chosen branch that will retract. Thus, the interneuron acts as a single-server queue to service each branch that is thus ordained. The state diagram for this model is depicted in Fig. 2 *D*, with single-server queue dynamics of forward transition probabilities, λ, and backward

TABLE 1 Model-based and experimental data-derived parameter estimates of the birth-death model of branching dynamics

	5 min				30 min
Time-interval	Birth rate	Death rate	Model-based	Empirical	Empirical
Treatment	λ (min^{-1})	μ (min^{-1})	ρ_m	ρ_e	ρ_e
Control	0.061	0.037	2.66	3.07	3.43
BDNF	0.102	0.032	4.15	4.16*	5.30†
Blebbistatin	0.043	0.026	2.66	3.00	3.03
NT-4	—	—	—	—	4.45†

Statistical analysis performed on data distributions from which these parameters are estimated.

*Test for the null hypothesis of equal cumulative distribution shape between treatments, KS-test, $p < 0.0001$.

†Test for the null hypothesis of equal group medians between treatments, KW-test, $p < 0.0001$.

transition probabilities, μ. For the control interneuron estimated rate parameters (Table 1), the birth rate, $\lambda = 0.061$, is greater than the death rate, $\mu = 0.037$. The model therefore predicts that the number of branches in the neuritic arbor grows unbounded over time, and no steady-state distribution of the number of branches exists (Fig. 2 *E*). This model of ordained branches is therefore discredited from modeling the branch dynamics.

The second hypothesized model is one of unrestricted branch retraction, that at any point in time, any of the existing branches may retract. Thus, the backward transition probabilities are state-dependent; for j branches in the arbor, the probability of transitioning to $j-1$ branches is given by $j\mu$, as in a dynamic multiserver queue where the number of servers equals the number of branches. The state diagram for this second model is depicted in Fig. 2 *F*. The steady-state branch distribution is derived from the flow-balance relations of the Kolmogorov equations and the fact that probabilities must sum to one,

$$(\lambda + j\mu)\pi_j = \lambda\pi_{j-1} + (j+1)\mu\pi_{j+1}, \tag{6}$$

$$\sum_{j=1}^{\infty}\pi_j = 1. \tag{7}$$

The solution is the Poisson distribution,

$$\pi_j = \frac{e^{-\rho}\rho^j}{j!}, \quad j \geq 0, \tag{8}$$

where parameter $\rho = \frac{\lambda}{\mu}$ is the mean number of branches in the neuritic arbor. An estimate of ρ, $\widehat{\rho}$, can be formed from the estimated birth and death rate parameters of the control interneurons, giving $\widehat{\rho} = 1.66$. Fig. 2 *G* plots the Poisson distribution parameterized by $\widehat{\rho}$, overlaid on the empirical pdf of the branch data. It is evident that this second model also provides an unsatisfactory fit to the experimental data.

The third model is derived from the observation that a migrating interneuron never exhibits less than one branch. We therefore build this into the model: the state diagram commences at state 1 and the number of branches that are available to retract in a neuritic arbor containing j branches is $j-1$. The resultant state diagram is shown in Fig. 2 *H*. The flow-balance equation, Eq. 6, is now

$$(\lambda + (j-1)\mu)\pi_j = \lambda\pi_{j-1} + j\mu\pi_{j+1}, \tag{9}$$

which, together with Eq. 7, has the solution of a shifted Poisson distribution,

$$\pi_j = \frac{e^{-(\rho-1)}(\rho-1)^{(j-1)}}{(j-1)!}, \quad j \geq 1, \tag{10}$$

where the mean number of branches, ρ, is now

$$\rho = \frac{\lambda}{\mu} + 1. \tag{11}$$

A model-based estimate of the mean number of branches, ρ, is formed from the estimated rates, as $\rho_m = \lambda/\mu + 1 = 2.66$. The shifted Poisson distribution parameterized by ρ_m is depicted in Fig. 2 *I*, well describing the experimental data.

For comparison with the model-based shifted Poisson distribution, an empirical distribution can also be formed by directly finding the best fit of Eq. 10 to the experimental data, with estimated parameter ρ_e. For the control interneurons, $\rho_e = 3.07$, which fits the data extremely well (Fig. 2 *C*) and is in good agreement with the ρ_m estimate (Table 1).

Stochastic model of branch dynamics encompasses perturbations

The branching dynamics were disrupted by treating cortical slices with either BDNF or blebbistatin. In this context, BDNF is known to be a positive guidance cue that directs interneurons into the cortex (8). We anticipated that perturbation of this directional cue would affect the movement and branching dynamics of interneurons. BDNF has also been described as a pro-branching factor that increases dendritic branching of cortical neurons (36,37), and therefore we hypothesized that the average neuritic arbor size would grow under the influence of BDNF. Blebbistatin, a specific myosin II ATPase inhibitor, is known to affect branching by disruption of actin-bundle turnover in growth cones (38) and by inhibition of nucleus displacement (13,39). Our a priori expectation on the likely effect of blebbistatin on the branching dynamics was that the disruption to nucleus movement and actin-bundle turnover would slow the turnover rate of branches in the neuritic arbor.

Both the BDNF and blebbistatin treatments induced striking but dissimilar changes to interneuron morphology (Fig. 1, *E* and *F*). Our hypothesis that the average neuritic arbor size would grow for interneurons cultured in the presence of BDNF ($n = 13$) could be achieved by a reduction in branch death rate (increase in lifespan) and/or an increase in branch birth-rate. The results displayed in Fig. 3, *A* and *C*, demonstrate that indeed both of these mechanisms occurred, with a 1.7-fold increase in branch interarrival rate and a 1.2-fold decrease in branch death rate compared to control (Table 1). In contrast to the BDNF treatment, blebbistatin-treated neurons ($n = 17$) caused a 1.4-fold decrease in birth rate and a 1.4-fold decrease in death rate (Fig. 3, *B* and *D*, and Table 1).

As with the control population, the estimates of ρ from the shifted Poisson distribution defining the steady-state distribution of the neuritic arbor can be calculated in two ways. Empirical estimates, ρ_e, can be calculated by directly fitting the shifted Poisson distribution (Eq. 10) to the experimental data (Fig. 3, *E* and *F*, and Table 1). Model-based estimates, ρ_m, can be estimated from the birth- and death-rate estimates using Eq. 11. The equilibrium distribution of branches computed using both ρ_e and ρ_m for the BDNF and blebbistatin treatments reveal an intriguing property of the branch

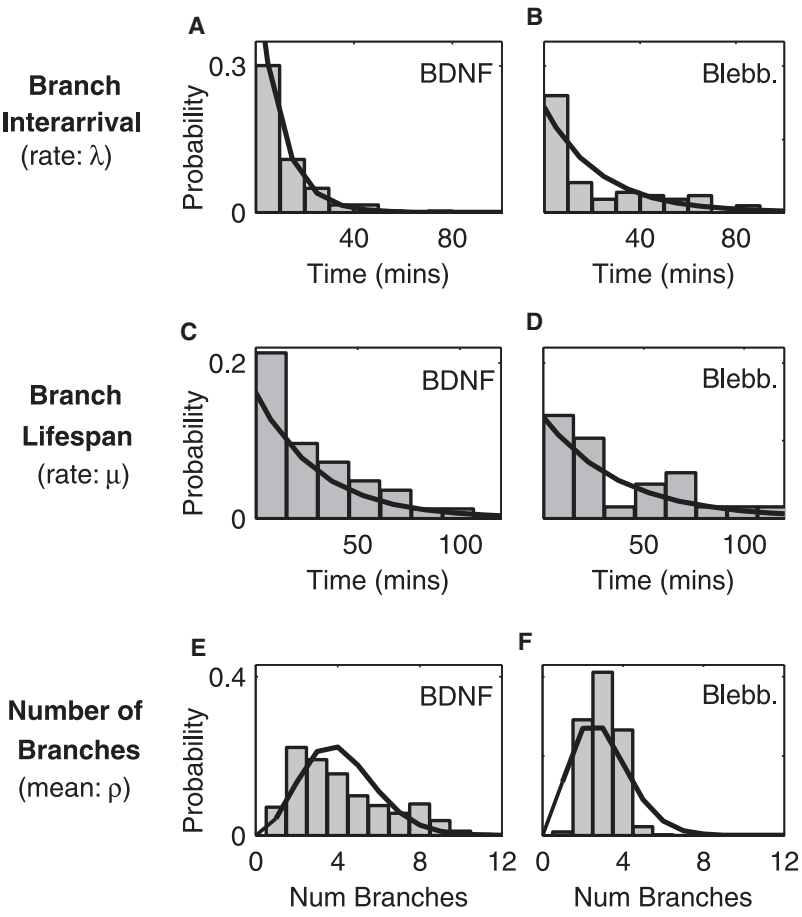

FIGURE 3 Birth-death model results for neurite branch dynamics in the presence of BDNF and blebbistatin. Histograms of branch interarrival times and best-fit exponential pdfs (Eq. 1, *solid lines*) for (*A*) BDNF and (*B*) blebbistatin. Histograms of branch lifespans and best-fit exponential pdfs (Eq. 2, *solid lines*) for (*C*) BDNF and (*D*) blebbistatin. Histograms of neuritic arbor size overlaid by empirically derived shifted Poisson distributions (Eq. 10, *solid lines*) parameterized by ρ_e for (*E*) BDNF and (*F*) blebbistatin.

dynamics. BDNF shows a 1.6-fold increase in neuritic arbor size, and a concomitant positive skew of the distribution, relative to control (Fig. 4). However, despite blebbistatin altering birth and death rates, the overall neuritic arbor size is conserved and is equivalent to that of the control neurons ($\rho_m^{Bleb}/\rho_m^{Cont} = 1.0075$ and $\rho_e^{Bleb}/\rho_e^{Cont} = 0.9772$; see Fig. 4).

Validation of the stochastic branch dynamics

Having demonstrated the utility of the birth-death process in modeling the branch dynamics under control and two perturbed experimental treatments, we tested the applicability of the same model to independent time-lapse sequences acquired at a different time interval. We analyzed images collected at 30-min intervals and constructed data distributions of the observed arbor size of neurons (Fig. S1). The longer imaging interval precluded accurate measurement of branch birth and death rates, as these processes occur on a faster timescale. Nonetheless, validation on this second dataset ensures that the modeling results are not a consequence of the original 5-min imaging protocol. We calculated pdf curves using the average branch numbers from the observed data and the shifted-Poisson model (Eq. 10). These pdfs are displayed over the histograms for control ($n = 44$; Fig. S1 *A*), BDNF ($n = 11$; Fig. S1 *B*), and blebbistatin-treated neurons ($n = 13$; Fig. S1 *C*). Of notable interest is the close agreement between the empirical pdfs and the data histograms, indicating that the birth-death model fits the 30-min imaging sequences well. Moreover, the ρ_e estimated from the 30-min data are in close agreement with the 5-min datasets (Table 1). These results indicate that the birth-death model robustly describes the branch dynamics displayed by both normal and perturbed migrating interneurons.

The observed responses of interneurons to BDNF do not differentiate between its role as a pro-branching factor and a guidance cue. To address this, we treated neurons with neurotrophin-4 (NT-4; $n = 20$), which is thought to affect only the guidance cue aspects of interneuron migration (8). The resultant 1.3-fold increase in the average branch number (Table 1) and positive skew of the branch number distribution (Fig. S1 *D*) can be attributed to the effect of the perturbed guidance cues without the confounding effect of altered branching mechanisms (40).

The conserved nature of nucleokinesis dynamics

Nucleus movement occurs in a saltatory fashion, with an initial strong acceleration progressing the nucleus in a leap, followed by a decreasing velocity as the nucleus reaches the final position. The observation of this form of motion

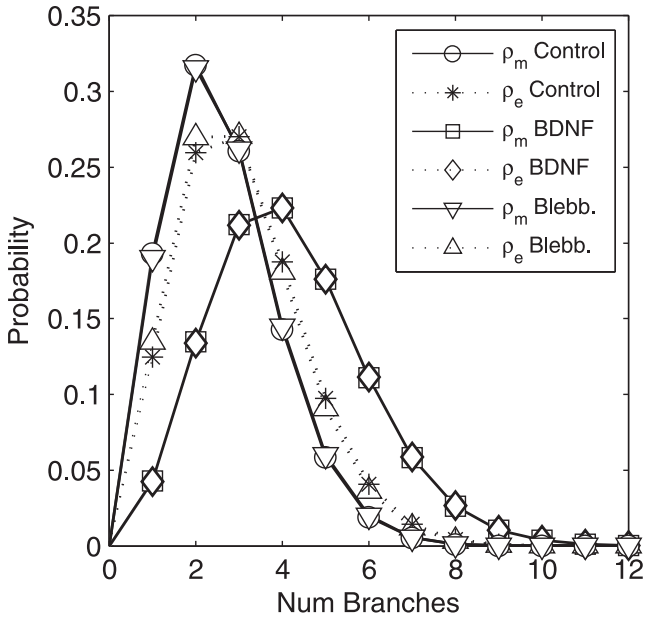

FIGURE 4 Comparison between empirically derived branch populations and model-based predictions. Probability distribution functions (Eq. 10) of average branch numbers derived from model-based and empirically-derived estimates, ρ_m and ρ_e, respectively. The BDNF distribution (KS-test, $p < 0.0001$) and median branch number (KW-test, $p < 0.0001$) are significantly different to control and blebbistatin.

suggested characterization of the nucleokinesis dynamics by a spring-dashpot system model (detailed in Methods). The trajectory of each nucleokinesis event, represented as accumulated distance, was calculated from the experimental data and is shown in Fig. 5 as solid lines for control ($n = 29$; Fig. 5 *A*), and as BDNF-treated ($n = 32$; Fig. 5 *B*). Only neurons tracked in the branching dynamics analysis were monitored for nucleokinesis events, thus allowing direct evaluation of alterations in neuritic arbor size.

The optimal spring-dashpot trajectory for each nucleokinesis event was determined using Eq. 5, shown as dotted lines for each nucleokinesis event in Fig. 5, *A* and *B*, in close agreement with the experimental data curves. The estimated parameters of each nucleokinesis event are plotted for the control and BDNF conditions in Fig. 5, *C* and *D*. There is no statistically significant difference in the estimated parameters for BDNF and control interneurons, as tested by Hotelling's T-square test. This suggests that despite perturbation of the neuronal arbor, once the nucleokinesis event is initiated, the nucleus moves with deterministic dynamics described by spring-dashpot parameters that are conserved across perturbations to branching. Interestingly, the estimated spring-dashpot parameters closely follow a critically damped system (*white lines*, Fig. 5, *C* and *D*). There were two control (of $n = 29$) and seven BDNF (of $n = 32$) outliers outside the range of these plots.

The timing of nucleokinesis events was not predictive of branch dynamics, as statistically analyzed by applying a Kolmogorov-Smirnov test to the distribution of time intervals between nucleokinesis events and branch births, and similarly branch deaths. No significant difference to a memoryless exponential distribution was found in either case (Fig. 6, *A–D*). We conclude that had nucleokinesis been predictive of branch dynamics, correlative structure would have been present. We examined in detail the displacement of leading neurite branches during nucleokinesis events. Two exemplar neurons undergoing nucleokinesis, one control and one BDNF-treated, were tracked across six image frames, as depicted in Fig. 6, *E* and *F*. The lengths of the asterisk-marked branches are plotted over time. These results clearly demonstrate a monotonic and linear increase in the length of the leading neurite branches through the nucleokinesis events.

DISCUSSION

The biological mechanisms by which cortical interneurons migrate from their birthplace in the medial ganglionic eminence to their final layered destinations in the developing cortex are of fundamental importance in brain development, as disruption to this process leads to a number of neurological disease states (1). The analyses of previous studies have been descriptive, providing information about the role of molecular guidance cues in migration. For example, interneurons are known to be attracted to certain molecular guidance cues, such as BDNF and NT-4, and repelled by other cues, such as slits (8–11,24). The use of organotypic slice cultures ensures that the interneurons are in as close to a realistic environment as is experimentally possible. Although there are limitations with this methodology, for example photobleaching and limited numbers of isolated cells, this is the current technology for this type of study.

Our study has investigated the relationship between two fundamental migration mechanisms—the branch dynamics and nucleokinesis of individual cells using high-resolution time-lapse confocal microscopy. Our primary observation regarding the branch dynamics is that the interneuron employs a stochastic search strategy, as branch interarrival and lifespan intervals were shown to be exponentially distributed. The memoryless property of the exponential distribution leads to the conclusion that the neuron's decision to extend and retract a branch is independent of previous branching history. The independence properties of interneuron branching were further elucidated by the evidence that a Markov chain model of the neuritic arbor in which a chosen or ordained branch retracts or splits to form a new branch is an unstable model without a steady-state solution that reflects the experimentally measured neuritic arbors. Instead, it was demonstrated that the best model is one in which all branches except one, are able to give rise to a branching or retraction event at any point in time. As observed experimentally, interneurons do not migrate without at least one branch.

Having derived a birth-death model in close agreement with the control interneuron data, we hypothesized the effect

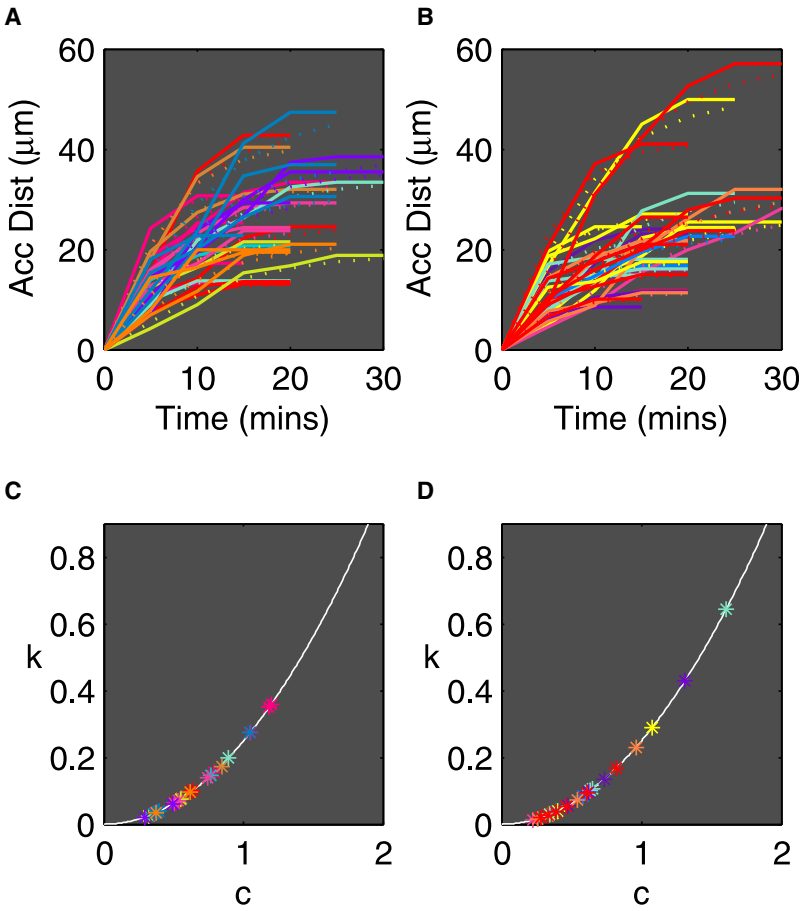

FIGURE 5 Nucleokinesis dynamics are unperturbed by branching disturbance. Plots show accumulated distance of nucleus movement over time from experimental data (*solid line*) and model-based predictions (*dotted line*) for (*A*) control and (*B*) BDNF-treated interneurons. Distribution of estimated parameters, k and c, for (*C*) control and (*D*) BDNF showing no significant difference between control and treatment (Hotelling's T-square test). Open lines depict critical damping, $k = c^2/4$.

of perturbing the system with BDNF and blebbistatin, two factors known to affect branching, and subsequently tested the model via experimental manipulation. The hypothesized increase in branch numbers predicted for the addition of BDNF was indeed reflected in the data, with the estimated model parameters displaying both an increase in branch birth and an increase in branch lifespan, indicating an increased stimulation of neurite formation, and that, on average, each neurite exists for a longer period. This is to be expected from neurons responding to a disruption of guidance cues or a pro-branching factor, both properties of BDNF (36,37). In contrast, blebbistatin decreased the branch birth rate and increased the branch lifespan, quantifying the notable morphological effects seen in the time-lapse experimental data where the branches of blebbistatin-treated neurons persist for longer periods of time. This is in agreement with Rösner et al., who demonstrated that blebbistatin causes elongation of neurites in chicken medulla neurons (41). Remarkably, however, the overall population dynamics of the neuritic arbor were conserved under application of blebbistatin, from which we speculate that interneurons have a preferred morphology that is maintained under perturbation to the cell mechanics, such as the disruption of actin-bundle turnover in growth cones caused by blebbistatin (38), but which is affected by explicit branching disturbances such as BDNF.

The validation of the stochastic branching model on independently acquired data with a 30-min imaging paradigm also provides clues regarding the mechanisms by which BDNF affects branch dynamics. It was shown that application of the extrinsic guidance cue NT-4 increased branch numbers to a lesser degree than BDNF. We hypothesize that it is the superposition of the intrinsic pro-branching and extrinsic guidance cue disturbances caused by BDNF that is responsible for the larger perturbation to preferred interneuron morphology than guidance cue disturbance alone.

The orthodox neurobiological view of the mechanisms of migration is that extracellular guidance cues are transmitted through intracellular signaling mechanisms to trigger the nucleus movement toward a chosen leading neurite (42). According to this notion, a one-to-one relationship between branching and nucleokinesis would predict perturbed migratory characteristics in response to changes in neuritic arbor size. Our results do not support this hypothesis. The BDNF treatment increased neuritic number, but there was no difference in the frequency of nucleokinesis events, or accumulated or net distances traveled (data not shown). What is evident from our analysis of nucleokinesis is that the dynamics of nucleokinesis are intrinsic to the interneuron. That is, once the choice of a leading neurite is

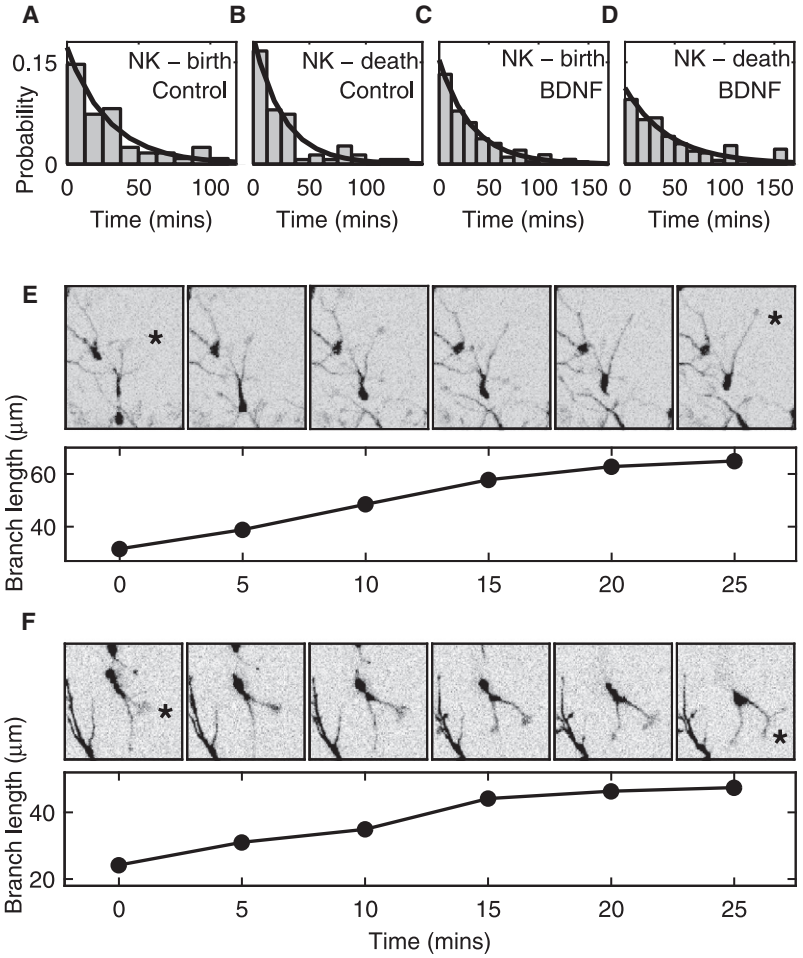

FIGURE 6 Relationship between branch dynamics and nucleokinesis. Histograms and best-fit exponential distributions of time intervals between nucleokinesis onset and branch (*A*) births and (*B*) deaths for control interneurons, and (*C*) births and (*D*) deaths for BDNF interneurons. Example of (*E*) a control interneuron and (*F*) a BDNF-treated interneuron undergoing nucleokinesis. The leading branch in each case (marked by * in *first* and *last frames*) grows throughout the nucleokinesis event.

made, the nucleus moves with conserved dynamics despite the degree of branching in the neuritic arbor.

The translocation of the nucleus along a chosen branch only as far as the stationary branch-point, where two branches fork, effectively isolates the nucleus movement from the branch extension and retraction. This reflects the motion of the microtubule-organizing center in shuttling between the soma and branch point (13,14). The weight of experimental evidence—including a counter-example demonstrating that, contrary to current opinion (13,25), the leading growth cone does not necessarily pause during nucleokinesis, and our model-based analyses—leads us to hypothesize that the temporal branching dynamics during interneuron migration can be considered in isolation from the events of nucleokinesis. Note that we do not claim that the event of branching itself is decoupled from nucleokinesis; signaling unequivocally occurs from the growth cones to the microtubule-associated proteins that coordinate the position of the microtubule organizing center and hence, soma (4,13). Our results do, however, clarify how nucleus movement and the temporal extension and retraction of branches can occur as independent processes (3). Future work will explore bottom-up models of nucleokinesis in the vein of previous biomechanical models of cell motility (22,23).

An analog stochastic search algorithm

We hypothesize that the interneuron branch dynamics perform an optimized and parallel stochastic search of the unexplored environment, as a biological analog of a Markov chain Monte Carlo (MCMC) method. MCMC algorithms are used to efficiently explore high-dimensional and multimodal probability density functions (43). From a given position in parameter space at which the pdf has been sampled, a random new position in the parameter space is drawn from a chosen proposal density, with the move accepted if the pdf at the new position exceeds the current pdf value, or with a nonzero probability otherwise. We postulate that the distribution of guidance cues in the substrate is analogous to a pdf, with attractive and repulsive zones forming the peaks and troughs of the pdf, respectively. Each growth cone samples the substrate and moves to a new position according to intrinsic rules of GC guidance (proposal density). Rather than a single sample at each time point as with a traditional MCMC method, the growth cones act as a parallel array of searching

mechanisms. Analogous to disconnected jumps in parameter space, abrupt changes in physical location are achieved by the emergence of new branches, enabling the search to further avoid being trapped in local minima or maxima.

Evidence in support of the stochastic search hypothesis is found in the memoryless properties of branch interarrival and lifespan and the corresponding Markov-chain branch population dynamics. Further evidence is provided by the persistent branching behavior of in vitro cultured interneurons removed from their natural environment (data now shown, and (13)). The supposition that an interneuron explores a novel area of the environment through the extension of a new branch, analogous to a jump in the parameter space of a MCMC search algorithm, is supported by recent work in which interneurons were shown to project a new branch in the direction of an attractive cue (25). Full experimental testing of the stochastic search hypothesis, however, requires that the substrate be able to be manipulated with precision, requiring both knowledge of substrate composition beyond that currently achievable, and the modification of an experimental assay for generating realistic molecular gradients (44).

Our study has focused on the dynamics of neurite branching. At the level of the growth cone, a similar analog stochastic search hypothesis has previously been posited. Modeled by a two-state random process with nonexponentially distributed states of growth and shrinkage (45,46), microtubule assembly and disassembly was hypothesized by Holy and Leibler (47) to form an efficient spatial search mechanism. This work was recently extended in an elegant simulation study (48), which further hypothesized the role of microtubule instability beyond postmigratory growth-cone pathfinding to cell motility.

In summary, our analysis of the dynamics of interneuron migration has revealed aspects of the process that both extend the results of traditional descriptive analyses and complement previous mathematical models of cell motility. Our results provide insight into the stochastic search mechanism at play in interneuron migration and the conserved, intrinsic nature of nucleokinesis and branching. Given future advances in experimental techniques, the models of temporal dynamics we have presented can be expanded to include the directional decision-making processes of migrating interneurons.

SUPPORTING MATERIAL

One figure and two movies are available at http://www.biophysj.org/biophysj/supplemental/S0006-3495(09)01018-2.

This work was supported by the National Health and Medical Research Council, Australia (to J.M.B. and S.-S.T.) and the Life Sciences initiative of the NICTA Victoria Research Laboratory (to L.A.J.).

REFERENCES

1. Ross, M. E., and C. A. Walsh. 2001. Human brain malformations and their lessons for neuronal migration. *Annu. Rev. Neurosci.* 24:1041–1070.
2. Friedl, P., and K. Wolf. 2003. Tumor-cell invasion and migration: diversity and escape mechanisms. *Nat. Rev. Cancer.* 3:362–374.
3. O'Rourke, N. A., M. E. Dailey, S. J. Smith, and S. K. McConnell. 1992. Diverse migratory pathways in the developing cerebral cortex. *Science.* 258:299–302.
4. Zheng, J. Q., and M. M. Poo. 2007. Calcium signaling in neuronal motility. *Annu. Rev. Cell Dev. Biol.* 23:375–404.
5. Araujo, S. J., and G. Tear. 2003. Axon guidance mechanisms and molecules: lessons from invertebrates. *Nat. Rev. Neurosci.* 4:910–922.
6. Guan, K. L., and Y. Rao. 2003. Signaling mechanisms mediating neuronal responses to guidance cues. *Nat. Rev. Neurosci.* 4:941–956.
7. Noctor, S. C., V. Martinez-Cerdeno, L. Ivic, and A. R. Kriegstein. 2004. Cortical neurons arise in symmetric and asymmetric division zones and migrate through specific phases. *Nat. Neurosci.* 7:136–144.
8. Polleux, F., K. L. Whitford, P. A. Dijkhuizen, T. Vitalis, and A. Ghosh. 2002. Control of cortical interneuron migration by neurotrophins and PI3-kinase signaling. *Development.* 129:3147–3160.
9. Pozas, E., and C. F. Ibanez. 2005. GDNF and GFRα1 promote differentiation and tangential migration of cortical GABAergic neurons. *Neuron.* 45:701–713.
10. Flames, N., J. E. Long, A. N. Garratt, T. M. Fischer, M. Gassmann, et al. 2004. Short- and long-range attraction of cortical GABAergic interneurons by neuregulin-1. *Neuron.* 44:251–261.
11. Tiveron, M. C., M. Rossel, B. Moepps, Y. L. Zhang, R. Seidenfaden, et al. 2006. Molecular interaction between projection neuron precursors and invading interneurons via stromal-derived factor 1 (CXCL12)/CXCR4 signaling in the cortical subventricular zone/intermediate zone. *J. Neurosci.* 26:13273–13278.
12. Alvarez-Buylla, A., and J. M. Garcia-Verdugo. 2002. Neurogenesis in adult subventricular zone. *J. Neurosci.* 22:629–634.
13. Bellion, A., J. P. Baudoin, C. Alvarez, M. Bornens, and C. Metin. 2005. Nucleokinesis in tangentially migrating neurons comprises two alternating phases: forward migration of the Golgi/centrosome associated with centrosome splitting and myosin contraction at the rear. *J. Neurosci.* 25:5691–5699.
14. Schaar, B. T., and S. K. McConnell. 2005. Cytoskeletal coordination during neuronal migration. *Proc. Natl. Acad. Sci. USA.* 102:13652–13657.
15. Dickinson, R. B., and R. T. Tranquillo. 1995. Transport equations and indices for random and biased cell migration based on single cell properties. *SIAM J. Appl. Math.* 55:1419–1454.
16. Rieu, J. P., A. Upadhyaya, J. A. Glazier, N. B. Ouchi, and Y. Sawada. 2000. Diffusion and deformations of single Hydra cells in cellular aggregates. *Biophys. J.* 79:1903–1914.
17. Dusenbery, D. 2001. Performance of basic strategies for following gradients in two dimensions. *J. Theor. Biol.* 208:345–360.
18. Shreiber, D. I., V. H. Barocas, and R. T. Tranquillo. 2003. Temporal variations in cell migration and traction during fibroblast-mediated gel compaction. *Biophys. J.* 84:4102–4114.
19. Ionides, E. L., K. S. Fang, R. R. Isseroff, and G. F. Oster. 2004. Stochastic models for cell motion and taxis. *J. Math. Biol.* 48:23–37.
20. Dieterich, P., R. Klages, R. Preuss, and A. Schwab. 2008. Anomalous dynamics of cell migration. *Proc. Natl. Acad. Sci. USA.* 105:459–463.
21. Satulovsky, J., R. Lui, and Y. L. Wang. 2008. Exploring the control circuit of cell migration by mathematical modeling. *Biophys. J.* 94:3671–3683.
22. Bottino, D., A. Mogilner, T. Roberts, M. Stewart, and G. Oster. 2002. How nematode sperm crawl. *J. Cell Sci.* 115:367–384.
23. Rubinstein, R., K. Jacobson, and A. Mogilner. 2005. Multiscale two-dimensional modeling of a motile simple-shaped cell. *SIAM Multiscale Model. Sim.* 3:413–439.
24. Metin, C., J. P. Baudoin, S. Rakic, and J. G. Parnavelas. 2006. Cell and molecular mechanisms involved in the migration of cortical interneurons. *Eur. J. Neurosci.* 23:894–900.
25. Martini, F. J., M. Valiente, G. L. Bendito, G. Szabó, F. Moya, et al. 2009. Biased selection of leading process branches mediates

chemotaxis during tangential neuronal migration. *Development*. 136: 41–50.

26. Graham, B. P., K. Lauchlan, and D. R. McLean. 2006. Dynamics of outgrowth in a continuum model of neurite elongation. *J. Comput. Neurosci*. 20:43–60.
27. Hely, T. A., B. Graham, and A. V. Ooyen. 2001. A computational model of dendrite elongation and branching based on MAP2 phosphorylation. *J. Theor. Biol*. 210:375–384.
28. Maskery, S. M., H. M. Buettner, and T. Shinbrot. 2004. Growth cone pathfinding: a competition between deterministic and stochastic events. *BMC Neurosci*. 5:22.
29. Xu, J., W. J. Rosoff, J. S. Urbach, and G. J. Goodhill. 2005. Adaptation is not required to explain the long-term response of axons to molecular gradients. *Development*. 132:4545–4552.
30. Varughese, M. M., and L. P. Fatti. 2008. Incorporating environmental stochasticity within a biological population model. *Theor. Popul. Biol*. 74:115–129.
31. Lee, Y., P. A. Markenscoff, L. V. McIntire, and K. Zygourakis. 1995. Characterization of endothelial cell locomotion using a Markov chain model. *Biochem. Cell Biol*. 73:461–472.
32. Atilgan, E., D. Wirtz, and S. X. Sun. 2005. Morphology of the lamellipodium and organization of actin filaments at the leading edge of crawling cells. *Biophys. J*. 89:3589–3602.
33. Britto, J. M., K. Obata, Y. Yanagawa, and S. S. Tan. 2006. Migratory response of interneurons to different regions of the developing neocortex. *Cereb. Cortex*. 16 (Suppl 1):i57–i63.
34. Tamamaki, N., Y. Yanagawa, R. Tomioka, J. Miyazaki, K. Obata, et al. 2003. Green fluorescent protein expression and colocalization with calretinin, parvalbumin, and somatostatin in the GAD67-GFP knock-in mouse. *J. Comp. Neurol*. 467:60–79.
35. Walsh, C. A., and A. M. Goffinet. 2000. Potential mechanisms of mutations that affect neuronal migration in man and mouse. *Curr. Opin. Genet. Dev*. 10:270–274.
36. Horch, H. W., and L. C. Katz. 2002. BDNF release from single cells elicits local dendritic growth in nearby neurons. *Nat. Neurosci*. 5:1177–1184.
37. Jin, X., H. Hu, P. H. Mathers, and A. Agmon. 2003. Brain-derived neurotrophic factor mediates activity-dependent dendritic growth in nonpyramidal neocortical interneurons in developing organotypic cultures. *J. Neurosci*. 23:5662–5673.
38. Medeiros, N. A., D. T. Burnette, and P. Forscher. 2006. Myosin II functions in actin-bundle turnover in neuronal growth cones. *Nat. Cell Biol*. 8:215–226.
39. Straight, A. F., A. Cheung, J. Limouze, I. Chen, N. J. Westwood, et al. 2003. Dissecting temporal and spatial control of cytokinesis with a myosin II Inhibitor. *Science*. 299:1743–1747.
40. Horch, H. W., A. Kruttgen, S. D. Portbury, and L. C. Katz. 1999. Destabilization of cortical dendrites and spines by BDNF. *Neuron*. 23: 353–364.
41. Rösner, H., W. Moller, T. Wassermann, J. Mihatsch, and M. Blum. 2007. Attenuation of actinomyosin II contractile activity in growth cones accelerates filopodia-guided and microtubule-based neurite elongation. *Brain Res*. 1176:1–10.
42. Tsai, L. H., and J. G. Gleeson. 2005. Nucleokinesis in neuronal migration. *Neuron*. 46:383–388.
43. Andrieu, C., N. D. Freitas, A. Doucet, and M. I. Jordan. 2003. An introduction to MCMC for machine learning. *Mach. Learn*. 50:5–43.
44. Rosoff, W. J., J. S. Urbach, M. A. Esrick, R. G. McAllister, L. J. Richards, et al. 2004. A new chemotaxis assay shows the extreme sensitivity of axons to molecular gradients. *Nat. Neurosci*. 7:678–682.
45. Odde, D. J., L. Cassimeris, and H. M. Buettner. 1995. Kinetics of microtubule catastrophe assessed by probabilistic analysis. *Biophys. J*. 69:796–802.
46. Odde, D. J., and H. M. Buettner. 1998. Autocorrelation function and power spectrum of two-state random processes used in neurite guidance. *Biophys. J*. 75:1189–1196.
47. Holy, T. E., and S. Leibler. 1994. Dynamic instability of microtubules as an efficient way to search in space. *Proc. Natl. Acad. Sci. USA*. 91:5682–5685.
48. Janulevicius, A., J. van Pelt, and A. van Ooyen. 2006. Compartment volume influences microtubule dynamic instability: a model study. *Biophys. J*. 90:788–798.